Wideband Planar Array With Integrated Feed and Matching Network for Wide-Angle Scanning

Justin A. Kasemodel, *Member, IEEE*, Chi-Chih Chen, *Senior Member, IEEE*, and John L. Volakis, *Fellow, IEEE*

***Abstract*—It is traditionally known that wideband apertures lose bandwidth when placed over a ground plane. To overcome this issue, this paper introduces a new non-symmetric tightly coupled dipole element for wideband phased arrays. The proposed array antenna incorporates additional degrees of freedom to control capacitance and cancel the ground plane inductance. Specifically, each arm on the dipole is different than the other (or non-symmetric). The arms are identical near the center feed section but dissimilar towards the ends, forming a ball-and-cup. It is demonstrated that the non-symmetric qualities achieve wideband performance. Concurrently, a design example for planar installation with balun and matching network is presented to cover X-band. The balun avoids extraneous radiation, maintains the array's low-profile height and is printed on top of the ground plane connecting to the array aperture with 180° out of phase vertical twin-wire transmission lines. To demonstrate the concept, a 64-element array with integrated feed and matching network is designed, fabricated and verified experimentally. The array aperture is placed $\lambda/7$ (at 8 GHz) above the ground plane and shown to maintain a active VSWR less than 2 from 8–12.5 GHz while scanning up to 70° and 60° in E- and H-plane, respectively. The array's simulated diagonal plane cross-polarization is approximately 10 dB below the co-polarized component during 60° diagonal scan and follows the theoretical limit for an infinite current sheet.**

***Index Terms*—Antenna feeds, broadband antennas, dipole antennas, phased arrays, planar arrays, scanning antennas, wide-angle scanning.**

I. Introduction

With space at a premium, there is strong interest to develop a single ultra wideband (UWB) phased array aperture, capable of concurrently supporting communications, electronic warfare and radar functions. Recent focus on conformal designs present new challenges for wideband apertures which commonly transform into narrowband or multiband configurations when placed on a ground plane. It is therefore not surprising that considerable attention has been given to electromagnetic bandgap (EBG) [1], [2] or frequency selective surfaces (FSS) [3] that mitigate the ground plane's destructive interference. However, EBGs, FSSs and other periodic ground planes are narrowband and not suited for wideband applications. Therefore, design of phased array apertures which are concurrently broadband and low-profile over a ground plane remains a challenge.

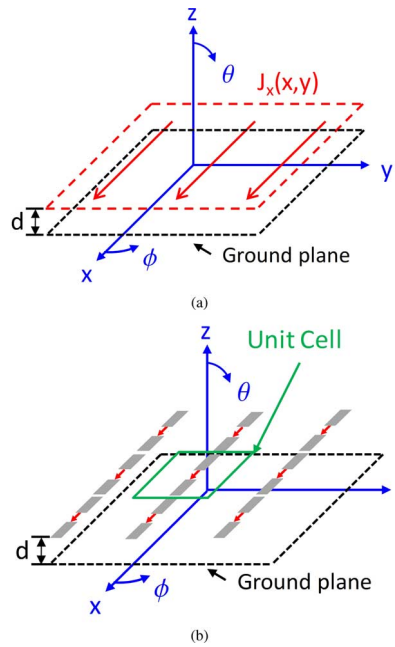

Fig. 1. (a) Infinite current sheet array over a ground plane and (b) tightly coupled dipole array implementation.

The infinite current sheet array (CSA) concept proposed by Wheeler [4] forms a theoretical basis for planar apertures. However, a broadband implementation was not realized in practice until Munk *et al.* [5], [6], emulated this concept using a tightly coupled dipole array (TCDA) as depicted in Fig. 1. An important aspect of TCDAs is the capacitive coupling between elements that enables the following: 1) allows field propagation to neighboring elements; 2) reduces dipole resonant frequency; 3) cancels inductive ground plane loading as a result of the strong capacitive coupling among dipole elements, yielding a low-profile, ultrawideband phased array aperture. The latter is critical for retaining the aperture's wideband behavior when placed in close proximately to a ground plane.

Previous wideband phased array antennas such as TEM-horn [7], body-of-revolution [8], bunny-ear [9], tapered slot, or Vivaldi [10] relied upon the third dimension of the element (depth), to achieve large bandwidths. As a result, they do not allow for conformal installations. They are also costly and difficult to fabricate.

Manuscript received July 28, 2011; revised December 14, 2012; accepted January 28, 2013. Date of publication June 04, 2013; date of current version August 30, 2013. Approved for Public Release 11- MDA-6271.

J. A. Kasemodel was with the ElectroScience Laboratory, Electrical and Computer Engineering Department, The Ohio State University, Columbus, OH 43212 USA. He is now with Raytheon Space and Airborne Systems, McKinney, TX 75071 USA (e-mail: justin.kasemodel@raytheon.com).

C-C. Chen and J. L. Volakis are with the ElectroScience Laboratory, Electrical and Computer Engineering Department, The Ohio State University, Columbus, OH 43212 USA (e-mail: chen.118@osu.edu; volakis@ece.osu.edu).

Color versions of one or more of the figures in this paper are available online at http://ieeexplore.ieee.org.

Digital Object Identifier 10.1109/TAP.2013.2266090

It is well understood that mutual coupling in an array can cause detrimental changes in performance such as element impedance variations, polarization degradation, and undesirable radiation patterns. In fact, mutual coupling is responsible for one of the more challenging aspects of phased array design, that of retaining uniform scan impedance. A fundamentally different design approach was proposed by Munk [5], where mutual coupling is used to lower the operational frequency and increase bandwidth. This approach is similar to designing wideband wide-angle FSSs [11]. Likewise, mutual coupling was shown to lower the operational frequency of a spiral array in [12].

Building on Munk's concept, in this paper, we present a new conformal array design that has several advantages: 1) inherently low-profile with good diagonal plane cross-polarization performance; 2) allows for conformal mounting on platforms (where a metallic ground plane is used); 3) employs planar element geometry for fabrication ease; and 4) enables significant cost reduction using planar printed circuit board (PCB) fabrication technology. The design is based on a infinite periodic array of dipoles modified to provide an increase in their design degree of freedoms. Specifically, the proposed non-symmetric geometry can be exploited for UWB or improved performance over a specific bandwidth. For the latter, a design is developed to operate over the entire X-band (8–12.5 GHz). A unique feature of the proposed array is its planar layered PCB construction. A single microwave laminate is used for the array aperture and another underneath supports all associated baluns and matching networks. For example, a 2166 element X-band array with associated baluns can be printed on two sheets of standard $(12 \text{ in} \times 18 \text{ in})$ PCB.

This paper is organized as follows. Section II introduces a novel non-symmetric element and provides a parametric study of its performance. A choice of parameters are then selected to achieve miniaturization and control input impedance. Section III presents a wideband feed providing impedance matching and balanced-to-unbalanced conversion (while maintaining the array's low-profile). The balun is printed on the array ground plane and connects to the array aperture using small twin-wire transmission lines. Section IV provides experimental demonstration using a 64 element (8×8) X-band array prototype. Section V showcases the array's diagonal cross-polarization performance and develops a fundamental limit on the diagonal plane cross-polarization ratio of planar current sheet apertures.

II. Non-Symmetric Array Element

The proposed non-symmetric dipole element unit cell is depicted in Fig. 2(a). Each arm is different than the other for better control of its self inductance and mutual capacitance with neighboring elements. The non-symmetric TCDA element is characterized by five variables; $t1$ (cup width), $t2$ (ball width), $t3$ (arm width), g (element separation gap), and α (cup opening angle). Below, we pursue a parametric study of these five geometric values with the TCDA unit cell width and distance (d) above the ground plane constant at 11.5 mm $(.5\lambda_H)$ and 8 mm

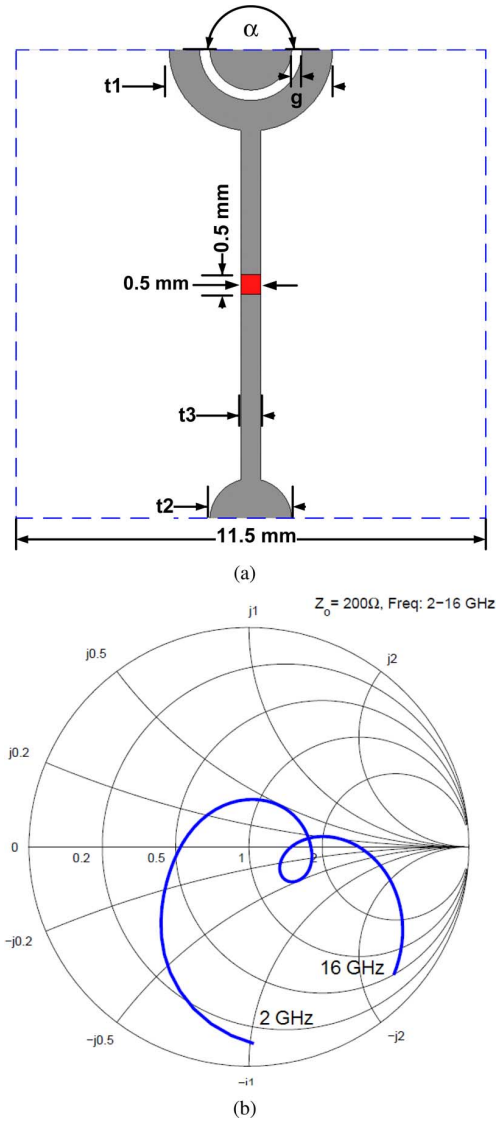

Fig. 2. Nonsymmetric element for TCDAs with $t1 = 2$ mm, $t2 = 1$ mm, $t3 = 0.5$ mm, $g = 0.254$ mm, $\alpha = 180°$ placed 8 mm above a ground plane. (a) Top view of the unit-cell geometry and (b) input impedance for broadside radiation normalized to $Z_o = 200\ \Omega$.

$(0.35\lambda_H)$, respectively, where λ_H is the free space wavelength at the highest design frequency of 13 GHz.

As a starting point, we chose the following parameters: $t1 = 2$ mm, $t2 = 1$ mm, $t3 = 0.5$ mm, $g = 0.254$ mm, $\alpha = 180°$. For this case the active input impedance is depicted in Fig. 2(b) as computed with infinite array analysis (periodic boundary conditions) using Ansoft's HFSS v12. Similar to [5] a nonsymmetric TCDA has a capacitive reactance at low frequencies which then passes through two resonances and two anti-resonances at higher frequencies forming a loop on the Smith chart. We note that a nonsymmetric TCDA has a broadside bandwidth of approximately 4.5:1 (active VSWR less than 2) which is similar to symmetric TCDAs found in the literature. The corresponding E- and H-plane scan element pattern (SEP), formally called the active element pattern [13], are shown in Fig. 3. This SEP includes the element pattern with all mutual coupling accounted for. Thus, the overall array pattern (ignoring edge effects) can be computed using the scan

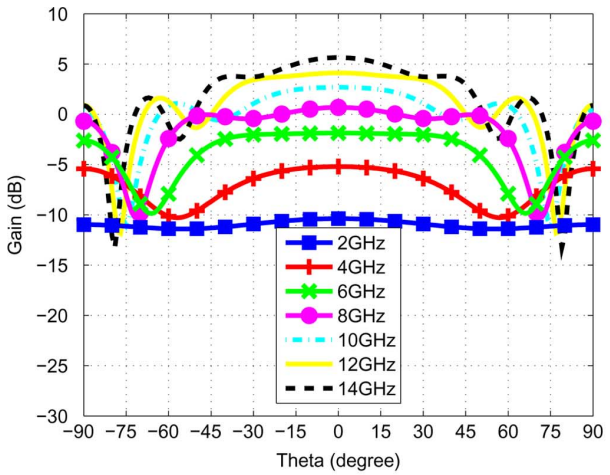

(a)

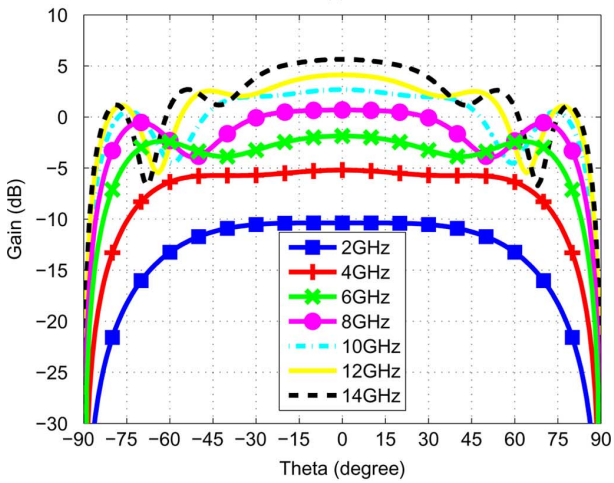

(b)

Fig. 3. Scan element pattern of the non-symmetric TCDA geometry in Fig. 2(a). (a) E-plane. (b) H-plane.

element pattern and array factor for a given finite array size and lattice [14].

From Fig. 3 we observe the E-plane SEP is similar to the H-plane pattern for $-45^\circ \leq \theta \leq 45^\circ$ and fairly constant over a broad range of frequencies. However, at low elevation angles (towards grazing) the E and H-plane patterns deviate substantially. Specifically, the E-plane pattern has sharper nulls, while the H-plane pattern vanishes at $\theta = \pm 90^\circ$. The latter is associated with cancellation of radiated fields along the horizon due to the ground plane image current. As expected, the boresight SEP ($\theta = 0^\circ$) is equal to the maximum unit cell directivity calculated by

$$D = \frac{4\pi A}{\lambda^2} \tag{1}$$

where A is the unit cell area. We remark that the SEP is typically stable with moderate geometry variations. Thus, we primarily focus on the scan impedance when designing the proposed broadband planar TCDA.

The first non-symmetric TCDA parameter to study is $t1$ (cup width). We found as $t1$ increases the low frequency reactance is reduced (a desirable effect). However, the resistance above

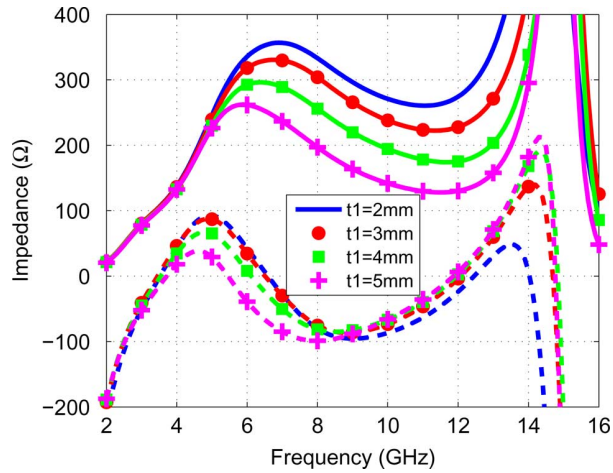

Fig. 4. Active resistance (solid) and reactance (dash) of the TCDA in Fig. 2(a) at broadside with $t1$ varied. All other parameters are kept constant: $t2 = 1$ mm, $t3 = 0.5$ mm, $g = 0.254$ mm, $\alpha = 180^\circ$.

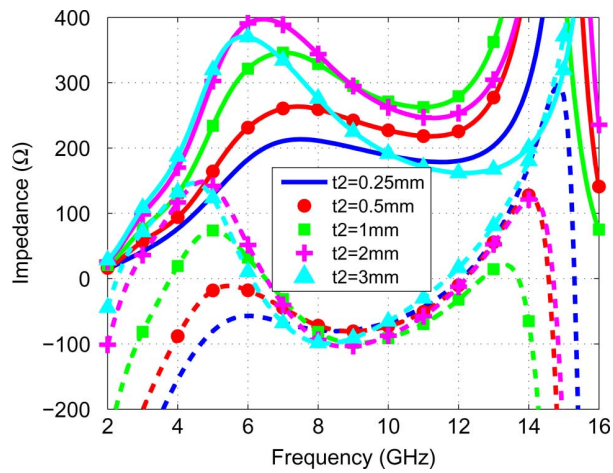

Fig. 5. Active resistance (solid) and reactance (dash) of the TCDA in Fig. 2(a) at broadside with the inner ball diameter ($t2$) varied and $t1 = t2 + g + 0.25$ mm. All other parameters are kept constant: $t3 = 0.5$ mm, $g = 0.254$ mm, $\alpha = 180^\circ$.

6 GHz is reduced as depicted in Fig. 4. Frequencies below 5 GHz are minimally effected.

To facilitate the study of $t2$ (the inner ball diameter), and not short the element to its neighbor, $t1$ had to also vary. Specifically, we set $t1 = t2 + g + 0.25$ mm, implying a constant 0.25-mm cup rim width. Fig. 5 shows the impedance of the TCDA as $t2$ was varied from 0.25 mm to 3 mm. We observe that $t2$ needs to be larger to lower the first resonance peak from 12 GHz down to 2.2 GHz when $t2 = 3$ mm. This is because as $t2$ increases, the capacitive junction area also increases, resulting in a larger mutual capacitance. As such, significant miniaturization is achieved (the lowest operational frequency is reduced).

The next parameter considered was the arm width or $t3$. As $t3$ increases, we observe a reduction of resistance and a larger reactance variation over the band (see Fig. 6). Below 5 GHz, the resistance is constant but for higher frequencies the resistance increases fourfold when decreasing the arm width to 3 mm from 0.5 mm. The larger resistance is attributed to a increased wire (self) inductance, also evident from the increased inductive reactance over the entire frequency range. As such, dipole arm

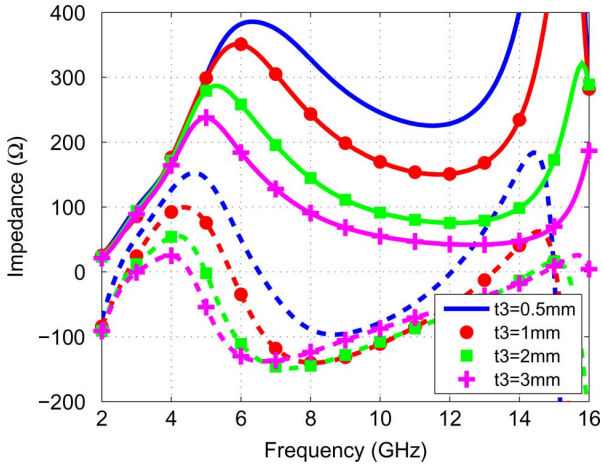

Fig. 6. Active resistance (solid) and reactance (dash) of the TCDA in Fig. 2(a) at broadside when $t3$ is varied. All other parameters are kept constant: $t1 = 2$ mm, $t2 = 1$ mm, $g = 0.254$ mm, $\alpha = 180°$.

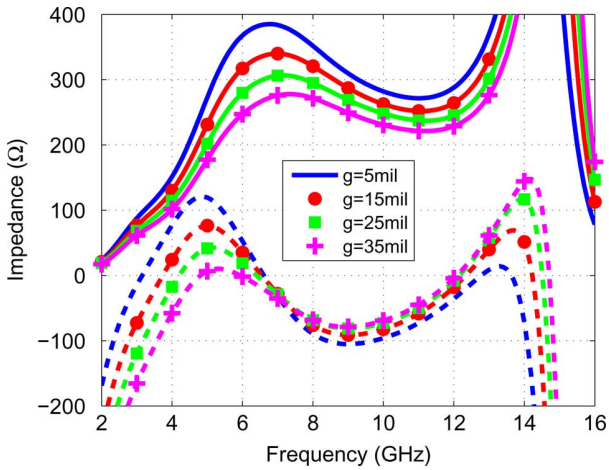

Fig. 7. Active resistance (solid) and reactance (dash) of the TCDA in Fig. 2(a) at broadside with the ball-and-cup gap (g) varied. All other parameters are kept constant: $t1 = 2$ mm, $t2 = 1$ mm, $t3 = 0.5$ mm $\alpha = 180°$.

width is an important parameter used to match the TCDA's radiation resistance to a specific system impedance.

Another important design parameter is the gap separating the ball and cup, g. When g is small, we expect a significant increase in mutual coupling (effectively miniaturizing the antenna). This also translates to a larger resistance at all frequencies. Concurrently, the operational bandwidth is shifted to lower frequencies. Fig. 7 does indeed show these effects. Therefore, we want to keep the gap separation as small as possible (i.e., within manufacturing tolerances) for broadband operation.

The final parameter considered is the cup opening angle α depicted in Fig. 8(a). Fig. 8(b) shows the impedance curves versus frequency for $\alpha = 45°$, $105°$, $165°$, $225°$, and $275°$. We observe that as α is reduced, coupling increases due to the larger capacitive area. This, of course, leads to the desired effect of lowering the frequency of operation. However, the resistance increases rapidly at 6 GHz making the array difficult to match over a broad frequency range given a constant system impedance, for example 200 Ω. Using the aforementioned impedance tuning results, the following parameters were selected for our X-band demonstration array: $t1 = 1.75$ mm, $t2 = 0.75$ mm, $t3 = 1$ mm, $g = 0.1778$ mm, and $\alpha = 85°$. This provides a fairly

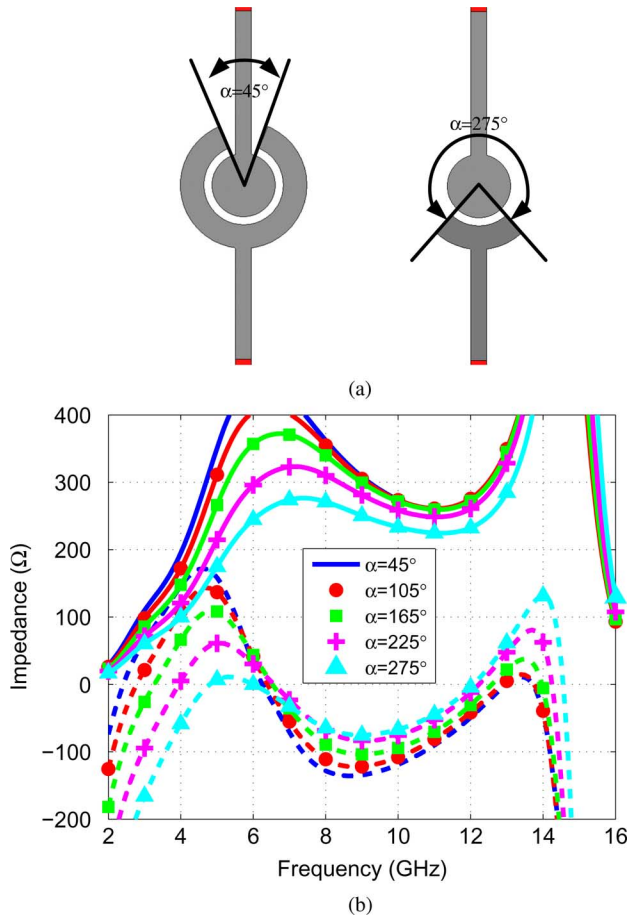

Fig. 8. Active impedance of the TCDA in Fig. 2(a) at broadside for varying α values. All other parameters are kept constant: $t1 = 2$ mm, $t2 = 1$ mm, $t3 = 0.5$ mm, and $g = 0.254$ mm. (a) Ball-and-cup geometry showing different α values. (b) Resistance (solid) and reactance (dash).

constant input impedance of ≈ 200 Ω with a small reactive component.

III. TCDA With Wideband Balun Feed

A wideband TCDA requires a wideband balanced feed for each element. As such, in [15] we designed, fabricated, and experimentally verified a small X-band prototype array with a wideband microstrip ring hybrid. The array had a single active element with remaining 63 elements terminated in 100-Ω resistors at the array aperture. The prototype array was used to examine some of the fabrication challenges and to validate numerical calculations. The hybrid employed coupled microstrip lines for bandwidth improvement [16]. However, further studies showed that the microstrip probe in [15] led to an increased cross-polarized field (only 10 dB below the copolarized component). We remark the array aperture without feed maintains a cross-polarized level 50 dB below copolarized gain in the principal planes. We therefore proceeded to minimize probe-ring coupling by relocating the probe location. The developed ring hybrid is shown in Fig. 9 and supports a 50-Ω coaxial input (GPO connector). The hybrid has two output ports extending inside the ring, 180° out of phase from each other producing the desired balanced feed. As a result, the fields add in series forming a 100 Ω balanced line. Unlike the design in [16], the

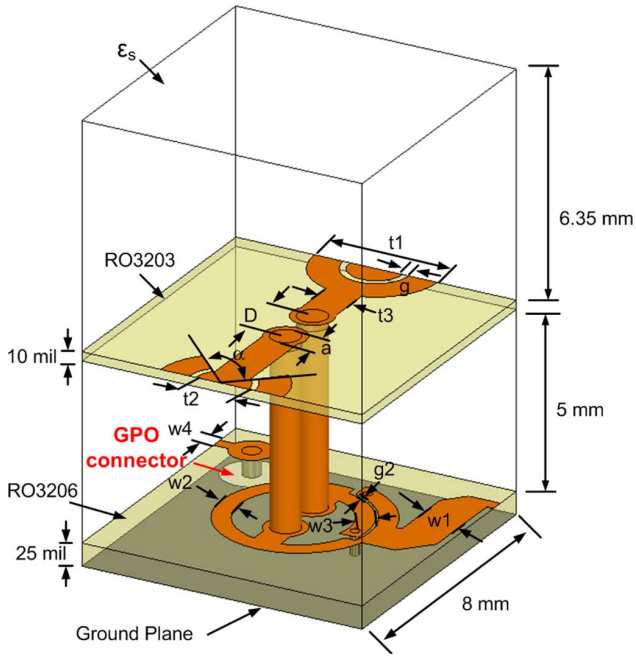

Fig. 9. Nonsymmetric TCDA unit cell geometry including the WAIM superstrate, integrated microstrip balun and twin wire matching network interconnects. The array parameters are given by: $t1 = 1.75$ mm, $t2 = 0.75$ mm, $t3 = 1$ mm, $g = 0.1778$ mm, $\alpha = 85°$, $a = 0.8128$ mm, $D = 1.4$ mm, $w1 = 1.2192$ mm, $w2 = 0.508$ mm, $w3 = 0.4318$ mm, $w4 = 0.3556$ mm, $g2 = 0.0762$ mm, and $\epsilon_s = 1.7$.

unused terminated sum or in-phase port was removed, reducing insertion loss by approximately 0.25 dB.

Due to the large array input resistance ($R_a \approx 200$ to 300 Ω for typical nonsymmetric TCDAs), the element cannot be directly connected to the 100-Ω ring output. Instead, a small twin-wire transmission line was used to connect and impedance match the array to the balun. Specifically, a twin-wire diameter and spacing of 0.8128 mm (20 gauge) and 1.4 mm, was used respectively. This yielded a characteristic impedance of 136 Ω, sufficient for our design while remaining easy to fabricate.

To avoid common-mode excitation typically found in tightly coupled arrays, the unit cell width and ground plane spacing was reduced to 8 mm and 5 mm, respectively. Reducing these dimensions shifts the common-mode above band. The common mode occurs when the antenna length and vertical feed lines are 1λ long. For more information on tightly coupled aperture common modes, the reader is referred to [17], [18]. In addition, a 6.35-mm-thick wide-angle impedance matching (WAIM) superstrate [19] having a dielectric constant (ε_s) of 1.7 was added to facilitate a wider scanning range. The non-symmetric element with integrated feed, microstrip hybrid and radome is shown in Fig. 9. Of importance is that the balun feed and array is printed using standard low-cost COTS PCB (Rogers 3203 for the array aperture and Rogers 3206 for the balun).

The boresight directivity and realized gain is shown in Fig. 10. We observe that the realized gain approaches the directivity from 8–12.5 GHz and cross polarization is less than −20 dB. Furthermore, the realized gain is within 0.3 dB of the maximum aperture directivity and the radiation efficiency is greater than 93% including dielectric and copper conductor losses. Of importance is the remarkable scanning performance

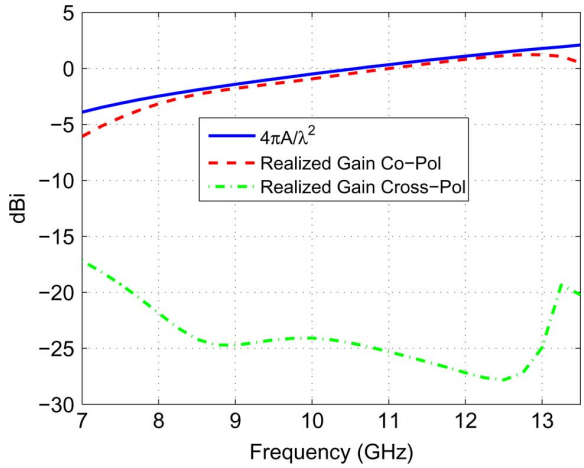

Fig. 10. Broadside realized gain of the non-symmetric TCDA unit cell with balun feed and WAIM radome.

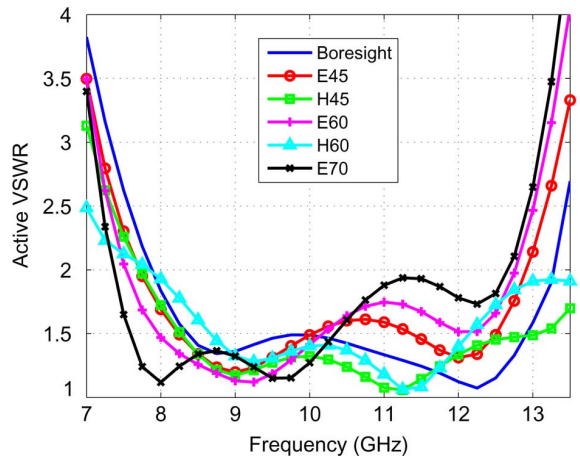

Fig. 11. Non-symmetric TCDA unit cell with feed active VSWR over multiple scan angles.

of this array. As depicted in Fig. 11, the array maintains an active VSWR less than 2 from 8–12.5 GHz while scanning up to 70° in the E-plane and 60° in the H-plane.

IV. 8 × 8 Finite Array Experimental Results

An 8 × 8 array was fabricated for measurements as depicted in Fig. 12. To realize this array, a solder mask was employed on the array and balun PCBs for soldering ease as shown in Fig. 12(b). In addition, each board was extended 12.7 mm around the array aperture to facilitate four nylon bolt holes. We also carried out finite array simulations using HFSS to serve as reference for the fabricated finite array prototype. We note that the only differences between fabricated and simulated geometries are the solder mask.

The array was mounted on a low permittivity dielectric pylon in the Electroscience Laboratory compact range. Fig. 13 displays the measured and simulated realized gain versus frequency for a single element (number 29) excited with all others terminated using 50-Ω GPO loads. The measured and simulated results are in good agreement, given the finite array simulation size with multiple dielectrics and detailed feed geometries. The simulation uses 1.83 million tetrahedra and memory usage of 61.1 GB.

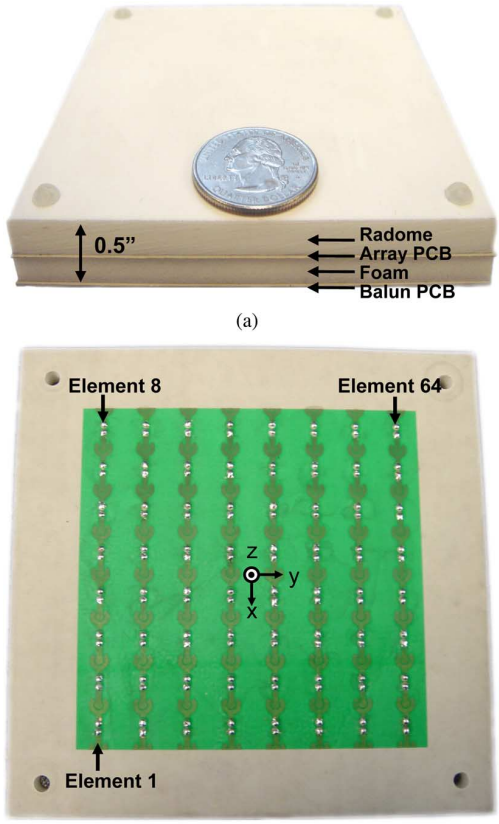

Fig. 12. X-band 64–element linear polarized array prototype. (a) With radome. (b) Radome removed.

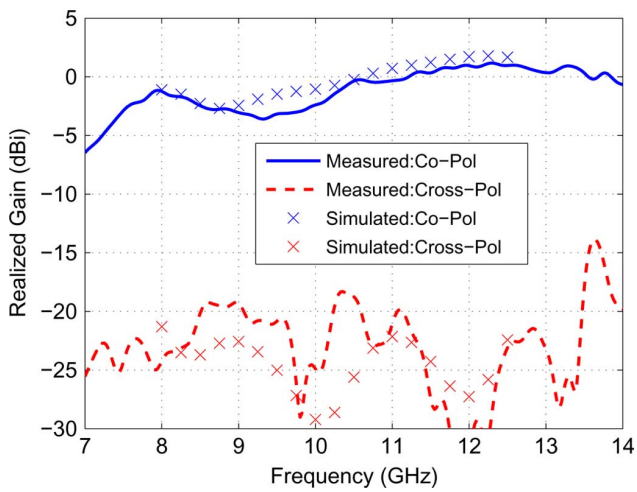

Fig. 13. Finite array broadside realized gain for a central element excited and remaining elements terminated in 50 Ω loads.

The E- and H-plane SEP for element 29 (near the array center) at 10 GHz (center frequency of the operating band) is shown in Figs. 14 and 15, respectively. The Ludwig third definition of cross-polarization is used [20], and found to be approximately −20 dB or lower over most of the principal plane scanning range. Due to the relative small size of the test array, edge effects dominate, therefore the SEP and active impedance of each element varies considerably [21]. As such, the increased level of cross-polarization near $\theta = 20°$ is not representative of the cross-polarization level while scanning. For more details on the

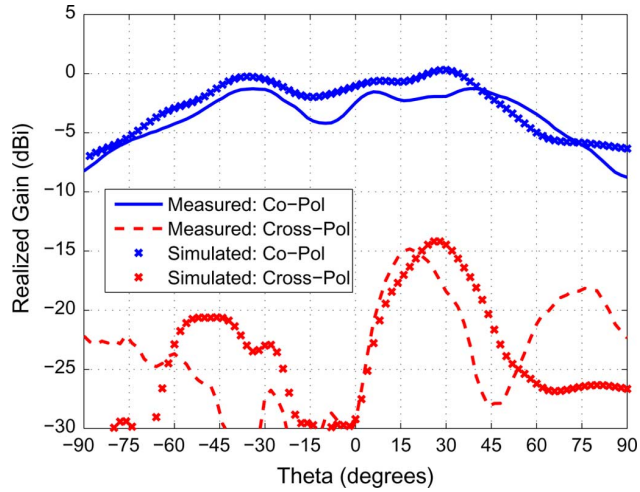

Fig. 14. Finite array E-plane SEP for a central element excited and remaining elements terminated in 50 Ω loads.

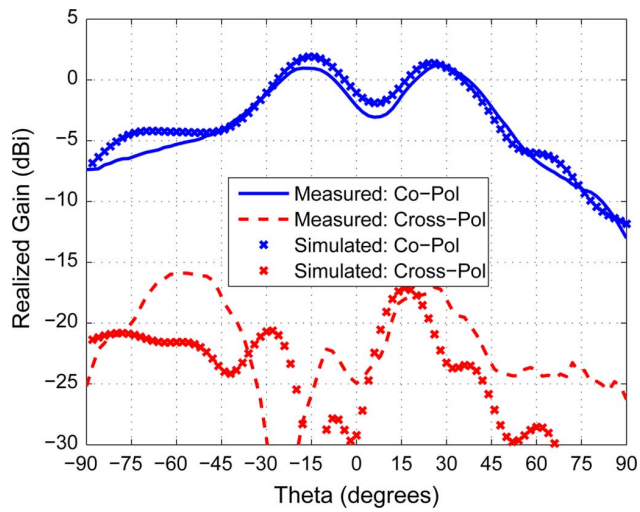

Fig. 15. Finite array H-plane SEP for a central element excited and remaining elements terminated in 50 Ω loads.

measured SEP variation and S-parameters across the aperture the reader is referred to [22]. The radiation patterns from 8 to 12.5 GHz show similar agreement and were omitted for brevity.

Of particular interest is the fully excited array gain and polarization level while scanning. To demonstrate the wide-angle scanning performance of the non-symmetric TCDA prototype, the radiation pattern of each element was measured and combined with uniform weighting using MATLAB. In addition, the array element excitations were progressively phased in simulation to steer the beam for numerical predictions.

The E-plane measured and simulated radiation pattern while scanning to broadside, 30° and 60° is shown in Fig. 16. Similarly, the H-plane beam steering performance is displayed in Fig. 17. We note that the simulated realized gain pattern incorporates the active (or scan) reflection coefficient mismatch for each element where the measured patterns (and subsequently post-processed combined pattern) uses the element's self reflection coefficient (S_{11}, S_{22}, etc.). Indeed, good agreement between simulated and measured scanning patterns in the principal planes are observed. The measured cross-polarized component is stronger than simulation predicted (not shown for clarity), but

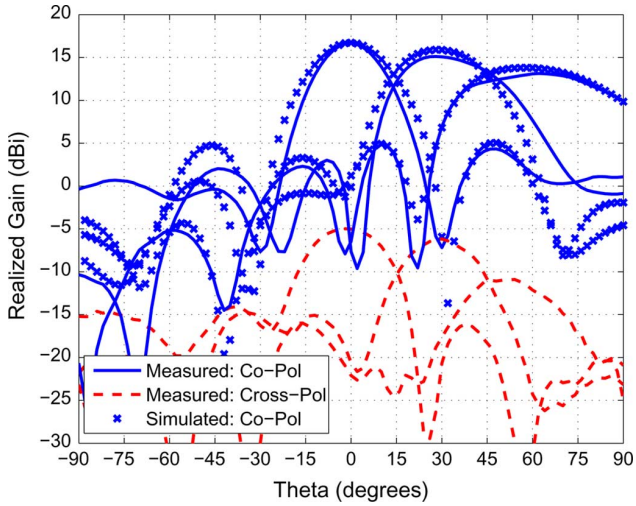

Fig. 16. Finite array E-plane radiation pattern at 10 GHz scanned to $\theta_o = 0°, 30°, 60°, \phi_o = 0°$.

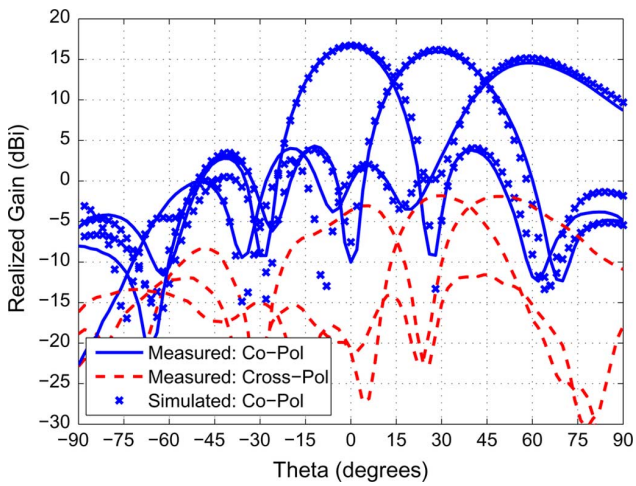

Fig. 17. Finite array H-plane radiation pattern at 10 GHz scanned to $\theta_o = 0°, 30°, 60°, \phi_o = 0°$.

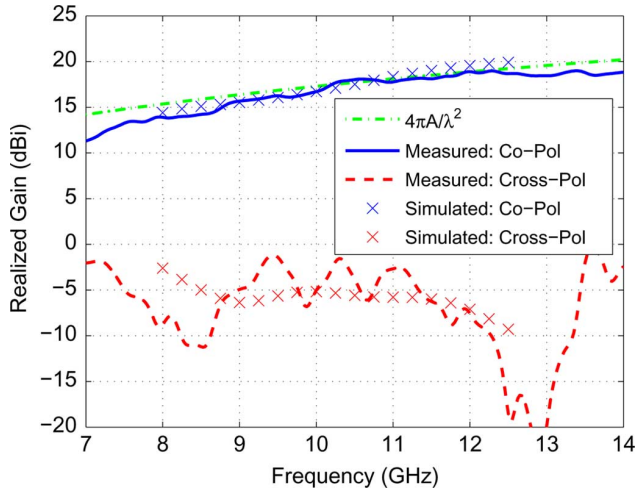

Fig. 18. Finite array broadside realized gain as a function of frequency with all elements excited.

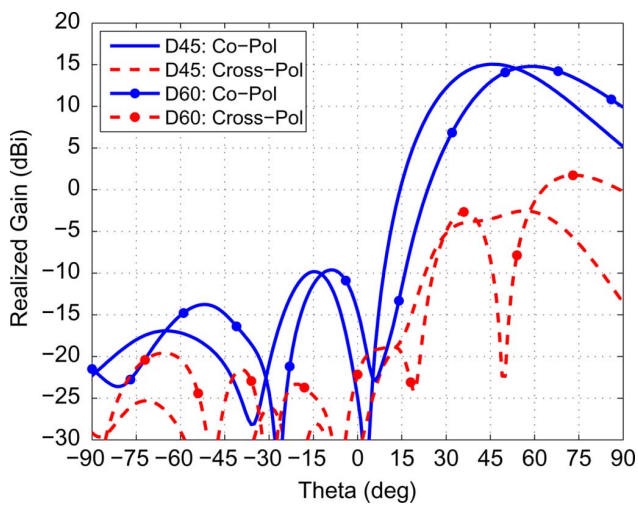

Fig. 19. Simulated finite array D-plane radiation pattern at 10 GHz scanned to $\theta_o = 45°, 60°, \phi_o = 45°$.

remains 18 dB below the copolarized component when scanned to 60° in the H-plane. It is believed that scattering from the array mounting fixture (as it is held by fiberglass attachments on the array's H-plane) contributes to the higher measured H-plane cross-polarized gain.

The measured and simulated broadside array gain is compared to the maximum theoretical directivity in Fig. 18. The simulated realized gain is higher than the theoretical limit above 11 GHz due to the finite ground plane diffraction adding in phase. Similarly, below 11 GHz the gain is slightly lower than the limit because the diffraction combines destructively. Further, we remark the area used in calculation was determined using the TCDA elements physical aperture area and not the PCB or ground plane area which extends past the aperture to accommodate mechanical mounting.

V. Diagonal Plane Cross-Polarization Performance

It is of interest to compare the developed non-symmetric TCDA to other wideband array technologies. A key feature of low-profile phased array antennas is the improved cross polarization ratio in the diagonal plane compared to traditional long UWB flared notch antenna designs [23], whose cross-polarization ratio can be positive (cross-polarization is stronger than the copolarized field) at wide scan angles.

First, we examined the D-plane cross-polarization ratio (E_x/E_y) using the 8×8 element finite array HFSS simulation model. The D-plane is defined as the diagonal plane $(\phi = 45°)$ and again the Ludwig third definition of polarization was used. The simulation model was scanned with uniform amplitude to 45° and 60°. As shown in Fig. 19, the diagonal plane cross-polarization level is approximately 15 dB below the copolarized component. The cross-polarization maximum at 60° scan is 12° further in angle than the co-polarized main beam. With this mind, the cross-polarization ratio was calculated using the maximum level of cross-polarization.

The theoretically achievable cross-polarization ratio of a uniform current sheet was calculated using (2) and (3) and serves as a reference level for the proposed non-symmetric dipole array:

$$E_x = E_\theta \cos\phi - E_\phi \sin\phi \tag{2}$$

$$E_y = E_\theta \sin\phi + E_\phi \cos\phi. \tag{3}$$

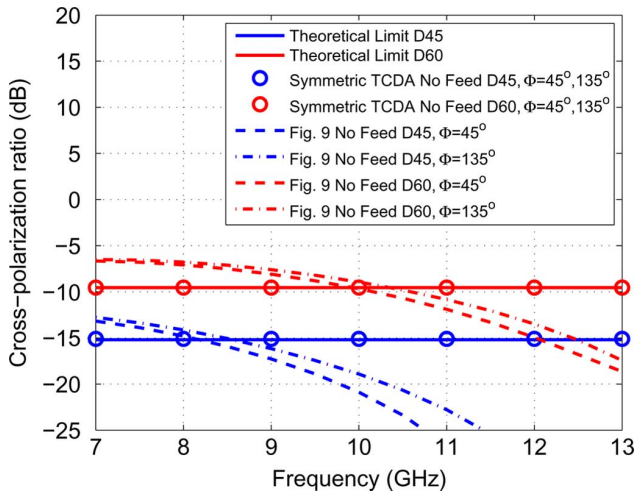

Fig. 20. Diagonal plane simulated infinite symmetric and non-symmetric TCDA without feed cross-polarization ratio scanned to $\theta_o = 45°, 60°$, $\phi_o = 45°$ and $135°$.

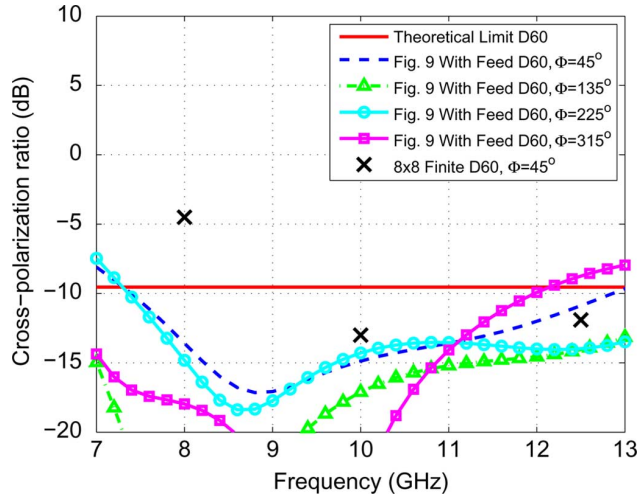

Fig. 21. Diagonal plane simulated infinite non-symmetric TCDA with feed and simulated 8×8 finite array cross-polarization ratio scanned to $\theta_o = 60°$.

An infinite uniform x-directed electric current sheet's radiated field components, E_θ and E_ϕ, are given by [24] and shown in (4) and (5). Note the factor $j\eta_o \exp\{-jk_o \cos\theta |z|\}$ was omitted where η_o is the intrinsic free-space wave impedance:

$$E_\theta = \cos\phi \tag{4}$$

$$E_\phi = \frac{-\sin\phi}{\cos\theta}. \tag{5}$$

Examining (2)–(5) it is clear the infinite current sheet polarization performance is not a function of frequency. To validate the formulation, a symmetric TCDA and the non-symmetric antenna in Fig. 9 was simulated without vertical twin-wire interconnects. A comparison between the theoretical cross-polarization limit is shown in Fig. 20. As expected, the symmetric element without feed is in perfect agreement with the limit and the nonsymmetric element is close. Due to the nonsymmetric structure, both $\phi_o = 45°$ and $\phi_o = 135°$ diagonal planes are shown. The element is symmetric with respect to the x-axis, therefore $\phi_o = 225°$ and $\phi_o = 315°$ is repetitive and omitted. The theoretical cross-polarization ratio of -15 dB at 45° D-plane scan is in agreement with [25] where a Greens function formulation was used. Further, the theoretical limit also agrees with other wideband planar phased array author's observations [26], [27]. Fig. 20 demonstrates that symmetric TCDAs and nonsymmetric TCDAs emulate an infinite current sheet.

The cross-polarization ratio for the design in Fig. 9 with feed is shown in Fig. 21. The element's cross-polarization level is above the theoretical curve at the band limits and below at the center portion of the band. This is a result of small feed radiation constructively and destructively canceling with the unwanted cross-polarized radiated field. For completeness, the simulated finite array cross-polarization ratio at $\phi_o = 45°$ and $\theta_o = 60°$ is plotted at the operational band's low, mid and high frequencies. The finite array diffraction also interferes with the antenna radiation and tracks the unit cell predicted response fairly well until 8 GHz when array truncation effects dominate.

VI. Conclusion

A novel nonsymmetric tightly coupled dipole array with integrated balun and matching network was presented. The array is placed $\lambda/7$ over a ground plane at the lowest frequency of operation (8 GHz). The array relied on a new non-symmetric dipole element offering several degrees of freedom to allow cancellation of the inductance caused by the ground plane. Multiple parametric sweeps were presented to control the array impedance and lower the frequency of operation. A wideband ring hybrid was proposed for unbalanced-to-balanced conversion. The feed is printed directly on the ground plane, maintaining the array's low-profile height and simple layered planar PCB construction. A 136-Ω twin wire transmission line connects the feed and aperture while providing impedance matching. We remark that the actual array bandwidth is much larger, and at this time is limited by the feed design. Future efforts will therefore focus on increasing feed bandwidth, to fully exploit the wide bandwidth enabled by this array concept. The developed ground plane backed array is capable of scanning up to 75° in E-plane and 60° in H-plane with an active VSWR less than 2 from 8–12.5 GHz (1.6:1). In the diagonal plane, the array's cross-polarization ratio agrees with a newly developed planar aperture theoretical limit of -15 dB and -9.5 dB at 45° and 60° scan, respectively. A small finite 8×8 array was fabricated and verified experimentally. Good agreement between simulation and measurement was confirmed over multiple scan angles.

Acknowledgment

The authors would like to thank N. Smith for help with array fabrication and measurement.

References

[1] F. Yang and Y. Rahmat-Samii, "Reflection phase characterizations of the EBG ground plane for low profile wire antenna applications," *IEEE Trans. Antennas Propag.*, vol. 51, no. 10, pp. 2691–2703, Oct. 2003.

[2] J. M. Bell, M. F. Iskander, and J. J. Lee, "Ultrawideband hybrid EBG/ferrite ground plane for low-profile array antennas," *IEEE Trans. Antennas Propag.*, vol. 55, no. 1, pp. 4–12, Jan. 2007.
[3] Y. E. Erdemli, K. Sertel, R. A. Gilbert, D. E. Wright, and J. L. Volakis, "Frequency-selective surfaces to enhance performance of broad-band reconfigurable arrays," *IEEE Trans. Antennas Propag.*, vol. 50, no. 12, pp. 1716–1724, Dec. 2002.
[4] H. Wheeler, "Simple relations derived from a phased-array antenna made of an infinite current sheet," *IEEE Trans. Antennas Propag.*, vol. AP-13, no. 4, pp. 506–514, Jul. 1965.
[5] B. A. Munk, *Finite Antenna Arrays and FSS*. New York, NY, USA: Wiley, 2003.
[6] B. A. Munk, R. Taylor, T. Durharn, W. Croswell, B. Pigon, R. Boozer, S. Brown, M. Jones, J. Pryor, S. Ortiz, J. Rawnick, K. Krebs, M. Vanstrum, G. Gothard, and D. Wiebelt, "A low-profile broadband phased array antenna," in *Proc. IEEE Antennas Propag. Int. Symp.*, Jun. 22–27, 2003, vol. 2, pp. 448–451.
[7] E. L. Holzman, "A wide band TEM horn array radiator with a novel microstrip feed," in *Proc. IEEE Int. Conf. Phased Array Syst. Technol.*, May 21–25, 2000, pp. 441–444.
[8] H. Holter, "Dual-polarized broadband array antenna with BOR-elements, mechanical design and measurements," *IEEE Trans. Antennas Propag.*, vol. 55, no. 2, pp. 305–312, Feb. 2007.
[9] J. Lee, S. Livingston, and R. Koenig, "A low-profile wide-band (5:1) dual-pol array," *IEEE Antennas Wireless Propag. Lett.*, vol. 2, pp. 46–49, 2003.
[10] J. Shin and D. H. Schaubert, "A parameter study of stripline-fed Vivaldi notch-antenna arrays," *IEEE Trans. Antennas Propag.*, vol. 47, no. 5, pp. 879–886, May 1999.
[11] B. A. Munk, *Frequency Selective Surfaces: Theory and Design*. New York, NY, USA: Wiley, 2000.
[12] H. Steyskal, J. Ramprecht, and H. Holter, "Spiral elements for broadband phased arrays," *IEEE Trans. Antennas Propag.*, vol. 53, no. 8, pp. 2558–2562, Aug. 2005.
[13] R. C. Hansen, *Phased Array Antennas*. New York, NY, USA: Wiley, 1988.
[14] D. Pozar, "The active element pattern," *IEEE Trans. Antennas Propag.*, vol. 42, no. 8, pp. 1176–1178, Aug. 1994.
[15] J. A. Kasemodel, C.-C. Chen, and J. L. Volakis, "Low-cost, planar and wideband phased array with integrated balun and matching network for wide-angle scanning," in *Proc. IEEE Antennas Propag. Soc. Int. Symp. (APSURSI)*, 2010, pp. 1–4.
[16] S. March, "A wideband stripline hybrid ring (correspondence)," *IEEE Trans. Microw. Theory Tech.*, vol. MTT-16, no. 6, pp. 361–361, Jun. 1968.
[17] D. Cavallo, A. Neto, and G. Gerini, "Common-mode resonances in ultra wide band connected arrays of dipoles: Measurements from the demonstrator and exit strategy," in *Proc. Int. Conf. Electromagn. Adv. Applicat. ICEAA'09*, 2009, pp. 435–438.
[18] D. Cavallo, A. Neto, and G. Gerini, "Analysis of common-mode resonances in arrays of connected dipoles and possible solutions," in *Proc. Eur. Radar Conf. EuRAD '09*, 2009, pp. 441–444.
[19] E. Magill and H. Wheeler, "Wide-angle impedance matching of a planar array antenna by a dielectric sheet," in *Proc. Antennas Propag. Soc. Int. Symp.*, Aug. 1965, vol. 3, pp. 164–169.
[20] A. Ludwig, "The definition of cross polarization," *IEEE Trans. Antennas Propag.*, vol. AP-21, no. 1, pp. 116–119, Jan. 1973.
[21] H. Holter and H. Steyskal, "On the size requirement for finite phased-array models," *IEEE Trans. Antennas Propag.*, vol. 50, no. 6, pp. 836–840, Jun. 2002.
[22] J. A. Kasemodel, C.-C. Chen, and J. L. Volakis, "Broadband planar wide-scan array employing tightly coupled elements and integrated balun," in *Proc. IEEE Int Phased Array Syst. Technol. (ARRAY) Symp.*, 2010, pp. 467–472.
[23] R. Kindt and D. Taylor, "Polarization correction in dual-polarized phased arrays of flared notches," in *Proc. IEEE Int. Symp. Antennas Propag. (APSURSI)*, Jul. 2011, pp. 1961–1964.
[24] A. Boryssenko, "Polarization constraints in dual-polarized phased arrays derived from an infinite current sheet model," *IEEE Antennas Wireless Propag. Lett.*, vol. 8, pp. 955–958, 2009.
[25] A. Neto, D. Cavallo, G. Gerini, and G. Toso, "Scanning performances of wideband connected arrays in the presence of a backing reflector," *IEEE Trans. Antennas Propag.*, vol. 57, no. 10, pp. 3092–3102, Oct. 2009.
[26] S. Holland and M. Vouvakis, "The planar ultrawideband modular antenna (PUMA) array," *IEEE Trans. Antennas Propag.*, vol. 60, no. 1, pp. 130–140, Jan. 2012.
[27] D. Cavallo, A. Neto, and G. Gerini, "A 10.5–14.5 GHz wide-scanning connected array of dipoles with common-mode rejection loops to ensure polarization purity," in *Proc. Antennas Propag. Society Int. Symp. (APSURSI)*, 2010, pp. 1–4.

Justin A. Kasemodel (S'05–M'10) received the B.S. degree in electrical engineering from South Dakota School of Mines and Technology (SDSMT), Rapid City, SD, USA, in 2006 and the M.S. and Ph.D. degrees in electrical engineering from The Ohio State University, Columbus, OH, USA, in 2009 and 2010, respectively.

Currently, he is a Principal Electrical Engineer at Raytheon Space and Airborne Systems, McKinney, TX. From 2004 to 2006, he was an Undergraduate Research Assistant at the Laboratory for Applied Electromagnetics and Communications, SDSMT. From 2006 to 2010, he was a Graduate Research Associate funded through a Northrop Grumman fellowship and Air Force Research Laboratory fellowship at The Ohio State University, ElectroScience Laboratory. In 2010, he joined Raytheon Space and Airborne Systems. His research interests include novel UWB antennas and phased arrays for military applications. At Raytheon, he has developed an IRAD and proprietary program portfolio where he is principal investigator or integrated product team leader developing innovative ultra wideband antennas, apertures and radomes. In general, he has developed emerging (TRL 2–6) antenna concepts (conformal, expendable, deployable, reconfigurable, survivable, miniature, thin, UWB, etc.) with 11 invention disclosures (three patents pending and two trade secrets) in nearly three years of employment.

Dr. Kasemodel is a member of Tau Beta Pi and Eta Kappa Nu. He was awarded second place at the 2006 IEEE Region 5 undergraduate student paper contest, third place at the 2008 Antenna Measurement and Techniques Association student paper contest and second place at the 2009 John D. and Alice Nelson Kraus Memorial student poster competition. He received the 2009 Antenna Applications Symposium best student paper award and was a recipient of the 2009 IEEE Antenna and Propagation Society doctoral research award. He was a student paper competition finalist at the 2010 IEEE International Symposium on Antennas and Propagation and received the best student paper award at the 2010 IEEE International Symposium on Phased Arrays Systems & Technology. He received the 2010 outstanding dissertation award at The Ohio State University ElectroScience Laboratory. Awards while at Raytheon include: two individual technical and one team achievement award, the Electronic Center 2012 "Big Idea" for technology being implemented today, 2012 Advanced Concepts and Technology Excellence award and 2012 technical honors rating.

Chi-Chih Chen (S'92–M'97–SM'07) received the M.S. and Ph.D. degrees from the Electrical and Computer Engineering Department, The Ohio State University, Columbus, OH, USA, in 1993 and 1997, respectively.

He has been with The Ohio State University ElectroScience Laboratory (ESL) since 1993 as a Postdoctoral Researcher (1997–1999), Senior Research Associate (1999–2003), and Research Scientist in (2004–2011). He is now a Research Associate Professor at The Ohio State University Electrical and Computer Engineering Department. His research interest are developing ultrawideband antennas, dielectric antennas, small antennas, GPS and GNSS antennas, body wearable antennas, phase array antennas, low-profile antenna arrays, directional finding arrays, RF power harvesting, ground penetrating radars, forward-looking GPR, vehicle obstacle detection radars, permittivity probes. He has published 45 journal papers, five book chapters, one coauthored book, and more than 80 technical reports.

Dr. Chen is an Edmund S. Gillespie Fellow of Antenna Measurement Techniques Association (AMTA), member of Society of Exploration Geophysicists,

Institute of Navigation. He served as Treasurer, Vice Chairman and Chairman of IEEE Joint AP/MTT Columbus from 2001 to 2003. He was Technical Chair of 2006 International Ground Penetrating Radar Conference. He is a member of the International Advisory/Science Committee of International Ground Penetrating Radar Conference since 2006. He served on the Technical Program Committee of 2011 IEEE APS/URSI Symposium. He is serving on the Technical Program Committee of 2013 IEEE Phase Array Symposium and Member-Elected Board of Directors of AMTA as the 2012 Technical Coordinator. He received OSU College of Engineering Lumley Research Award in 2004 and 2010. He is also a member of Sigma Xi and Phi-Kappa-Phi.

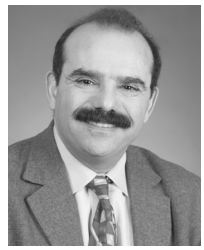

John L. Volakis (S'77–M'82–SM'89–F'96) was born in Chios, Greece, on May 13, 1956. He received the B.E. degree (*summa cum laude*) from Youngstown State University, Youngstown, OH, USA, in 1978 and the M.Sc. and Ph.D. degrees from The Ohio State University, Columbus, OH, USA, in 1979 and 1982, respectively.

He started his career at Rockwell International (1982–1984), now Boeing. In 1984, he was appointed Assistant Professor at The University of Michigan, Ann Arbor, MI, USA, becoming a Full Professor in 1994. He also served as the Director of the Radiation Laboratory from 1998 to 2000. Since January 2003, he has been the Roy and Lois Chope Chair Professor of Engineering at The Ohio State University and also serves as the Director of the ElectroScience Laboratory. Over the years, he carried out research in antennas, wireless communications and propagation, computational methods, electromagnetic compatibility and interference, design optimization, RF materials, multi-physics engineering, bioelectromagnetics, terahertz, and medical sensing. His publications include eight books [among them: *Approximate Boundary Conditions in Electromagnetics* (IEE, 1995) *Finite Element Methods for Electromagnetics* (IEEE Press, 1998) *Antenna Engineering Handbook, Fourth Edition* (McGraw-Hill, 2007), *Small Antennas* (McGraw-Hill, 2010), and *Integral Equation Methods for Electromagnetics* (SciTech, 2012)], over 320 journal papers, nearly 600 conference papers and 23 book chapters. He has graduated/mentored over 70 doctoral students/post-docs with 20 of them receiving best paper awards at conferences.

Prof. Volakis was 2004 President of the IEEE Antennas and Propagation Society, twice the general Chair of the IEEE Antennas and Propagation Symposium, IEEE APS Distinguished Lecturer, IEEE APS Fellows Committee Chair, IEEE-wide Fellows committee member and Associate Editor of several journals. He is listed by ISI among the top 250 most referenced authors (2004), and is a Fellow of ACES. Among his awards are: The University of Michigan College of Engineering Research Excellence award (1993), Scott award from The Ohio State University College of Engineering for Outstanding Academic Achievement (2011) and the IEEE AP Society C-T. Tai Teaching Excellence award (2011).